Subduction of trench-fill sediments beneath an accretionary wedge: insights from sandbox analogue experiments

Atsushi Noda[1,1], Hiroaki Koge[1,1], Yasuhiro Yamada[2,2], Ayumu Miyakawa[3,3], and Juichiro Ashi[4,4]

[1]National Institute of Advanced Industrial Science and Technology
[2]JAMSTEC
[3]Geological Survey of Japan, AIST
[4]University of Tokyo

November 30, 2022

Abstract

Ancient exhumed accretionary complexes are sometimes associated with high-pressure–low-temperature (HP–LT) metamorphic rocks, such as psammitic schists, which are derived from sandy trench-fill sediment. At accretionary margins, sandy trench-fill sediments are rarely subducted to the depth of HP metamorphism because they are commonly scraped off at the frontal wedge. This study uses sandbox analogue experiments to investigate the role of seafloor topography in the transport of trench-fill sediment to depth during subduction. The experiments were conducted with a detached, rigid backstop to allow a topographic high (representing a seamount) to be subducted through a subduction channel. In experiments without topographic relief, progressive thickening of the accretionary wedge pushed the backstop down, leading to a stepping down of the décollement, narrowing the subduction channel, and underplating the wedge with subducting sediment. In contrast, in experiments with a topographic high, the subduction of the topographic high raised the backstop, leading to a stepping up of the décollement and widening of the subduction channel. These results suggest that the subduction of topographic relief is a possible mechanism for the transport of trench-fill sediment from the trench to HP environments through a subduction channel. A sufficient supply of sediment to the trench and topographic relief on the subducting oceanic plate might enable trench-fill sediment to be accreted at various depths and deeply subducted to become the protoliths of HP–LT metamorphic rocks.

Subduction of trench-fill sediments beneath an accretionary wedge: insights from sandbox analogue experiments

Atsushi Noda*[1], Hiroaki Koge†[2], Yasuhiro Yamada[3], Ayumu Miyakawa[1], and Juichiro Ashi[2]

[1]Geological Survey of Japan, National Institute of Advanced Industrial Science and Technology (AIST), Central 7, Higashi 1-1-1, Tsukuba, Ibaraki 305-8567, Japan

[2]Atmosphere and Ocean Research Institute, The University of Tokyo, 5-1-5 Kashiwanoha, Kashiwa-shi, Chiba 277-8564, Japan

[3]Japan Agency for Marine-Earth Science and Technology (JAMSTEC), 3173-25 Showa-machi Kanazawa, Yokohama 236-0001, Japan

December 18, 2019

ABSTRACT

Ancient exhumed accretionary complexes are sometimes associated with high-pressure–low-temperature (HP–LT) metamorphic rocks, such as psammitic schists, which are derived from sandy trench-fill sediment. At accretionary margins, sandy trench-fill sediments are rarely subducted to the depth of HP metamorphism because they are commonly scraped off at the frontal wedge. This study uses sandbox analogue experiments to investigate the role of seafloor topography in the transport of trench-fill

*E-mail: a.noda@aist.go.jp

†Current address: Geological Survey of Japan, National Institute of Advanced Industrial Science and Technology (AIST), Central 7, Higashi 1-1-1, Tsukuba, Ibaraki 305-8567, Japan

sediment to depth during subduction. The experiments were conducted with a detached, rigid backstop to allow a topographic high (representing a seamount) to be subducted through a subduction channel. In experiments without topographic relief, progressive thickening of the accretionary wedge pushed the backstop down, leading to a stepping down of the décollement, narrowing the subduction channel, and underplating the wedge with subducting sediment. In contrast, in experiments with a topographic high, the subduction of the topographic high raised the backstop, leading to a stepping up of the décollement and widening of the subduction channel. These results suggest that the subduction of topographic relief is a possible mechanism for the transport of trench-fill sediment from the trench to HP environments through a subduction channel. A sufficient supply of sediment to the trench and topographic relief on the subducting oceanic plate might enable trench-fill sediment to be accreted at various depths and deeply subducted to become the protoliths of HP–LT metamorphic rocks.

INTRODUCTION

High-pressure–low-temperature (HP–LT) metamorphic rocks derived from terrigenous sedimentary rocks are known to occur at subduction margins. Such metamorphic rocks are exposed alongside low-grade accretionary rocks and fore-arc basin strata that include coarse-grained sandy deposits with the same depositional ages as the metamorphic rocks. For example, the Sanbagawa Metamorphic Complex in southwestern Japan contains HP–LT psammitic and even conglomeratic schists (e.g., Wallis, 1998), and the depositional ages and geochemical characteristics of the protolith are almost identical to those of sandstone from the low-grade Shimanto Accretionary Complex (Kiminami et al., 1999; Shibata et al., 2008; Aoki et al., 2012) and submarine fan turbidites deposited in the associated fore-arc basin (Noda and Sato, 2018) (Figure 1). These observations indicate that terrigenous trench-fill sediments were accreted in a shallow subduction zone and were also subducted to >20 km depth. Other examples of such subduction–accretion-related HP–LT metamorphic rocks can be seen in the Franciscan Complex in California (e.g., Ernst, 2011; Jacobson et al., 2011; Dumitru et al., 2015; Raymond, 2018), the Chugach terrane in Alaska (Plafker et al., 1994), the Central

Pontides in Turkey (Okay et al., 2006), and the Coastal Cordillera in Chile (Glodny et al., 2005; Willner et al., 2004; Angiboust et al., 2018).

At typical sedimentary accretion zones, such as those in Cascadia (Gulick et al., 1998; Booth-Rea et al., 2008; Calvert et al., 2011), Alaska (Moore et al., 1991; Ye et al., 1997), Java (Kopp et al., 2009), southern Chile (Glodny et al., 2005; Melnick et al., 2006), Sumatra (Singh et al., 2008; Huot and Singh, 2018), and Japan (Park et al., 2002; Kimura et al., 2010), terrigenous trench-fill sediments are generally scraped off at the frontal wedge, whereas hemipelagic-to-pelagic sediments underplate the base of the accretionary wedge (e.g., Scholl, 2019). This may be because the increased structural thickness of the wedge and progressive dewatering of subducting sediment causes the décollement to step down and narrow the subduction channel (e.g., Sample and Moore, 1987; Vannucchi et al., 2008). This suggests that the growth of the accretionary wedge might inhibit the subduction of terrigenous sediment beyond the wedge through the subduction channel. However, occurrences of HP–LT metasandstone at some accretionary margins demonstrate that terrigenous sediment can be subducted beneath the wedge. One hypothesis is that a topographic high enables trench-fill sediment to be subducted under the wedge (Figure 2). Subducting seamounts followed by subducting material can be observed beneath the wedge along accretionary margins in southwestern Japan (Moore et al., 2014), Alaska (Li et al., 2018), Barbados (Moore et al., 1995), and Hikurangi (Barker et al., 2009; Bell et al., 2010).

The subduction of terrigenous material associated with the rough topography of a subducting oceanic plate has been proposed to explain tectonic erosion of the wedge (e.g., von Huene and Culotta, 1989; Lallemand et al., 1994; von Huene et al., 2004). Sandbox analogue experiments have shown the potential for sediment transport below the frontal wedge behind a subducting topographic high (Lallemand et al., 1992; Dominguez et al., 2000). Numerical simulations show that in the wake of a subducting seamount, there are unfaulted strata, large-offset thrust faults, increased fault spacing, an oversteepened surface slope, and intense deformation along the base of the wedge (Morgan and Bangs, 2017). In addition, recent seismic profiles across the accretionary margins of the Nankai Trough (Bangs et al., 2006) and the Hikurangi Trench (Bell et al., 2010) reveal that subducting seamounts or ridges and the surrounding sediment are accommodated by a step-up in the décollement, and the surrounding sediment is being transported to depth.

However, the influence of a subducting seamount beneath an accretionary wedge on subduction and accretion fluxes is not well understood. In particular, the role of topographic highs in modifying the décollement level and in maintaining or rejuvenating the subduction channel as a conduit for sediment subduction needs to be explored. The purpose of this study is (1) to investigate how the topographic roughness of the subducting plate interface influences material fluxes, including the accretion of sediment to the wedge and the subduction of sediment along the subduction channel, and (2) to propose a model that explains how terrigenous trench-fill sediment can be transported to depth. We performed two types of sandbox analogue experiment, one with and one without a topographic high. The novelty of these experiments is that they used a detached backstop to reproduce the subduction and underplating of sediment when a rigid topographic high is subducted beneath an accretionary wedge. We also inserted two weak layers within the sand, to reproduce the situation where the subducting sediment includes several potential slip surfaces. Such multiple décollements are commonly found within underthrust sediments or at the top of the oceanic crust, including at the Nankai (Moore et al., 2001; Park et al., 2002), Hikurangi (Ghisetti et al., 2016; Plaza-Faverola et al., 2016), and Barbados (Saffer, 2003) accretion zones.

METHODS

Model Setup and Experimental Materials

A scaled 2-D analogue modeling technique was used for this study so that the results could be compared with naturally occurring geological structures (e.g., Buiter, 2012; Graveleau et al., 2012). A glass-sided rectangular deformation rig with internal dimensions of 100 cm $\times$ 30 cm $\times$ 20 cm was used (Figure 3). A steel plate was positioned at one end as a fixed wall with a small open window at the bottom. A rigid wedge made from wood was placed next to the steel plate but was not fixed to it. The wedge was designed to behave like a static backstop that has a higher mechanical strength than the accretionary wedge (e.g., Tsuji et al., 2015). A rigid backstop is used to ensure stability during the experiments and for repeatability. The mobility of the backstop helped to replicate the deformable nature of equivalent structures in natural geological systems, and to allow topographic relief to be subducted. The backstop had a surface slope that dips at 30° and is covered by sandpaper. A plastic (Mylar®) sheet was placed over the rig's base plate and fixed to a roll that pulled the sheet using a stepper motor (on the left side in Figure 3). The sheet was pulled beneath the rigid backstop at a rate of 0.5 cm/min, thereby compressing the experimental material above.

Two types of granular material were used for the experiments: Toyoura sand and glass micro-beads. Dry granular materials like these are widely used as analogue materials to simulate the brittle and frictional behavior of sedimentary rocks in accretionary wedges because they display elastic–frictional plastic behavior and reproduce the non-linear deformation of crustal rocks under brittle conditions (e.g., Dahlen, 1984; Lohrmann et al., 2003; Graveleau et al., 2012). Toyoura sand, a standard testing material commonly used by Japanese civil engineers, is a spherical quartz-rich sand with a particle size of 0.14–0.26 mm (D_{50} = 0.2 mm), a density of approximately 1600 kg m^{-3}, an internal coefficient of friction, μ, of 0.59–0.68, and a cohesion, C, of 105–127 Pa (Yamada et al., 2006; Dotare et al., 2016). The glass micro-beads are spherical and 0.045–0.063 mm in diameter, have a low internal coefficient of friction (μ = 0.47) and low cohesion (40 Pa), and are considered a suitable analogue for weaker layers (Yamada et al., 2006, 2014).

Layers of sand and glass micro-beads with a total thickness of 3.4 cm were used in the experiments. The sand and glass were sprinkled into the rig from a height of approximately 30 cm above the rig floor (Figure 3). Alternating layers of blue, red, and black sand were laid down to help visualize the cross-sectional geometry of the models, without influencing the mechanical homogeneity. Mechanically weak layers were created by adding two thin layers of glass micro-beads, each 3 mm thick.

Experiment A (Exp. A) investigated the subduction of a smooth oceanic plate beneath a static backstop (Figure 3a). Experiment B (Exp. B) investigated the subduction of topographic relief (e.g., a seamount), using a block that was attached to the plastic sheet (Figure 3b). The height of the relief was 1.6 cm, approximately half of the total thickness of the sediment. The height of the relief was chosen to avoid drastic deformation of the accretionary wedge. The surface of the topographic relief was covered by a Teflon® sheet. The total amount of horizontal shortening was 30 cm for Exp. A and 35 cm for Exp. B.

After each 2 cm increment of shortening, we sprinkled dry sand from at least 10 cm above the surface of the accretionary wedge to fill the topographic lows that had developed (Figure 4). This sand was used to replicate sedimentation in fore-arc/slope basins that form on the surfaces of accretionary wedges. A total of 1129 g of sand was added over the course of Exp. A and 910 g during Exp. B. The volumes of sand added during Exp. A and B were 706 and 569 cm^3, respectively.

In addition to investigating wedge morphology, we studied temporal variations in sediment influx/outflux. The sediment influx and outflux (cm^2) were calculated using the thicknesses (cm) of the trench-fill sediments (influx) and the subduction channel underneath the backstop (outflux), which were multiplied by the rig width (30 cm) and divided by the length of shortening (cm). Input and output (cm^3) are here defined to be the integrals of influx and outflux, respectively, with respect to shortening length (cm). Time-lapse digital images were taken through the transparent side glass at 5 s intervals using a PC-based controller. The images were later analyzed to calculate sediment influx/outflux and to study the cross-sectional geometry of the wedges. The experiments did not account for the effects of isostatic compensation and erosion, which would have contributed to the differences between our models and natural examples (e.g., Schellart and Strak, 2016).

Scaling

Models used in laboratory experiments should be properly scaled so that the results can be considered true analogues of geological processes (e.g., Hubbert, 1937). It is assumed that brittle deformation will obey frictional Mohr–Coulomb-type laws. The basic scaling relationship between the physical properties of a model and those in nature, which relates the stress, σ, density, ρ, gravity, g, and length, l (Hubbert, 1937; Schellart, 2000) is

$$\frac{\sigma_g}{\sigma_m} = \frac{l_g}{l_m} \times \frac{g_g}{g_m} \times \frac{\rho_g}{\rho_m}. \tag{1}$$

where the subscripts m and g indicate model and geological values, respectively. The cohesion C can substitute for stress, σ (Schellart, 2000; Graveleau et al., 2012), and the experiments are performed under normal gravity ($g_m/g_g = 1$); consequently, Eq. 1 can be modified to give

$$\frac{l_g}{l_m} = \frac{C_g}{C_m} \times \frac{\rho_m}{\rho_g}. \tag{2}$$

For mean bulk density values of 2000–2500 kg m^{-3} and cohesion values of 5–20 MPa, which are typical of sedimentary rocks in accretionary wedges (Schumann et al., 2014), the length scale ratio ranges from approximately 3×10^4 to 1×10^5. A 1 cm model layer in an experiment therefore corresponds to 300 m to 1 km in nature. The 3.4-cm-thick sediment layers used in this experiment can be scaled to 1–3 km of strata, which is a moderate thickness of trench-fill sediment for a modern accretionary margin (Noda, 2016). The 5 cm width and 1.6 cm height of the topographic relief used in Exp. B can be scaled to 1.5–5 km and 0.5–1.6 km, respectively. The scaled dimensions of the topographic relief are comparable to many seamounts on the Pacific plate. However, the height-to-radius ratio of 0.64 in the model is higher than that of 0.21 for natural seamounts (Jordan et al., 1983; Smith, 1988). This high ratio is used to enhance the effects of topography. The total amount of shortening during the experiments was 30–35 cm, which is equivalent to 9–35 km of displacement. Assuming a plate convergence rate of 5 cm/year, this in turn corresponds to 1.8–7 $\times 10^5$ years. A sediment supply to the topographic lows of 910–1129 g for 6×10^5 years is equivalent to a sediment budget on the order of 10^6 t/year. The calculated sediment budget is the same order of magnitude as the sediment load in many mountainous rivers in Japan and New Zealand (Milliman and Syvitski, 1992), and the sedimentary influx into the Kumano Basin during the last 4 Myr (50 km $\times$ 70 km $\times$ 2 km).

RESULTS

Experiment A: Subduction without a seamount

During the first ~9 cm of shortening, high-frequency, low-amplitude forethrusts developed in front of the backstop (Stage 1, Figure 5a; 8 cm of shortening in Figure 6). The wedge was uplifted quickly (uplift rate is 0.34 in Figure 5d), and thus the slope increased rapidly, exceeding 12° by the end of Stage 1 (Figure 5c). After the emergence of T_6 (Stage 2), the frequency of forethrust initiation and the uplift rate of the wedge (0.10) were lower than during Stage 1, but the rate of wedge widening (0.22) remained nearly constant (Figure 5). The slope of the wedge surface ranged from 8.5° to 13°, and was 9.5° at the end of the experiment (Figure 5c).

Deformation was concentrated in the upper layer of glass beads, which acted as a décollement, until 16 cm of shortening (Figure 6). At around 18 cm of shortening the décollement stepped down to the lower layer of glass beads as the toe of the backstop subsided below the upper layer of glass beads. During this stage, the footwall of forethrust T_7 underthrust the wedge and the sand layer between the two layers of glass beads underplated the wedge, creating a duplex structure (18–24 cm of shortening in Figure 6). This underthrusting raised the hanging wall of T_7 and created a piggy-back basin (trench-slope basin) on top of the wedge (22 cm of shortening). After the activation of T_8, with the lower layer of glass beads acting as a décollement, subducting sediment was accreted to both the frontal and basal parts of the wedge with increasing amount of underplating and thickness of the forethrust sheet of T_8. The final forethrust, T_9, was initiated with the upper layer of glass beads acting as the detachment (30 cm of shortening). The final wedge was nearly 30 cm in length and had a constant slope of 9.5° (Figure 5). The toe of the backstop further subsided, to the lower layer of glass beads (30 cm of shortening in Figure 6).

The outflux from the subduction channel (sediment subduction) gradually decreased, but its rate of change increased (Figure 5e). In particular, after the décollement stepped down, the outflux dropped rapidly. Influx to the accretionary wedge (solid dashed line in Figure 5e) increased to balance the total sediment influx. The output-to-input ratio of the experiment was 0.36 (Table 1).

Experiment B: Subduction With a Seamount

Stage 1 of Exp. B was almost identical to that of Exp. A in terms of wedge progradation, and the widening and uplift rates of the wedge (Figure 5a–d). Stage 2 started after the initiation of forethrust T_5, earlier than in Exp. A. T_5 was active for over 12.8 cm of shortening, exceeding that of any other forethrust in either experiment (Figure 5a). This long activity acted to reduce the width of the wedge and steepened its slope to 17.7° (Figure 5b, c). The wedge progradation rate during Stage 2 was 0.10, nearly half that of Exp. A (Figure 5a). The uplift rate varied from 0.06 to 0.29, but the mean rate was the same as in Exp. A (Figure 5b).

The wedge deformation process during Stage 1 of Exp. B was similar that in Exp. A (0–6 cm of shortening in Figure 7). However, at 7 cm of shortening, the seamount triggered the first forethrust of Stage 2 at 10 cm from the toe of the wedge (T_5 in Figure 7). The subduction of the seamount led to an undeformed layer underthrusting the wedge, and then uplifted the hanging wall as a trench-slope basin to create accommodation space (10–16 cm of shortening in Figure 7).

A décollement was formed in the upper layer of glass beads on the landward side of the seamount and in T_5 on the trenchward side during the period between the initiation of T_5 and collision of the seamount with the backstop (8–12 cm of shortening in Figure 7). Just prior to the collision (12–18 cm of shortening), both the upper and lower layers of glass beads were sliding and the sand layer between two layers of glass beads underplated and was injected into T_5. The décollement stepped up from the lower layer of glass beads to T_5 when the seamount passed. In addition, following the collision the seamount raised the backstop and opened a subduction channel beneath it (>20 cm of shortening in Figure 7). The subsequent forethrusts, T_6 and T_7, were rooted in a décollement in the upper layer of glass beads. Finally, the toe of the backstop subsided slightly, causing the lower layer of glass beads to act as a décollement.

Sediment outflux gradually decreased (blue line in Figure 5f), as it did during Exp. A, until the seamount reached the backstop. After the seamount raised the backstop, at around 17–20 cm of shortening (Figure 7), sediment outflux fully recovered and even exceeded its initial rate (Figure 5d). Outflux soon decreased again as the seamount subducted farther landward and the backstop subsided (Figure 5f). The output-to-input ratio of the experiment was 0.46 (Table 1).

DISCUSSION

Décollement Step-down and Underplating

The gradual decrease of the outflux in Exp. A (Figure 5e) increased the influx to the accretionary wedge, which increased its growth rate. During the time the upper layer of glass beads acted as a décollement, the sediment above it was accreted to the wedge front. As the slip switched to the lower layer of glass beads, the sediment between the two layers of glass beads underplated the wedge, and frontal accretion continued. Similar results have been reported in previous analogue experiments; i.e., underplating becomes significant when the outflux from the subduction channel (sediment subduction) is smaller than the influx (Kukowski et al., 1994; Albert et al., 2018). The results of our experiment support the conclusion that a narrowing of the subduction channel and a decrease in outflux can lead to sediment underplating the wedge and faster wedge growth.

If we assume that sand above the upper layer of glass beads is terrigenous sediment, and that sand below this layer is hemipelagic–pelagic sediment, the former can be scraped off at the wedge front and the latter may be underplated below the wedge (see Figure 8). This occurs because terrigenous and hemipelagic sediments tend to be detached as a result of variations in diagenetic alteration (Moore, 1975) or smectite content (Vrolijk, 1990; Deng and Underwood, 2001), or existence of weak smectitic pelagic clay (Moore et al., 2015). This can be observed in the Nankai Trough, where there is a step-down in the décollement at 1–3 km depth, in the transitional region between the aseismic and seismic zones (cf. Park et al., 2002; Kimura et al., 2007), which could be due to the different physical properties of these rock types.

The stepping down of the décollement in this study was associated with subsidence of the backstop, which was probably linked to increased overburden stress caused by thickening of the wedge. Increased overburden stress may inhibit the subduction of terrigenous sediment to great depth. Underplating related to subsidence of the backstop (inner wedge) also occurs along erosive margins. For example, thick (> 2 km) sediment cover suggests subsidence of the inner wedge of the Ecuador–Colombia margin (Collot et al., 2008). Seismic profiles indicate underplating between listric splay faults and the basal décollement beneath the apex of the inner wedge, but the total mass flux at the plate interface is negative (Collot et al., 2008), and material at the base of the inner wedge is eroded.

Décollement Step-up and Sediment Subduction

In Exp. B, the subduction of a seamount shifted the décollement from the glass bead layers into forethrust T_5 along the leading flank of the seamount. While T_5 was active as a "top décollement" (cf. Lallemand et al., 1994), incoming undeformed layered sand in the wake of the seamount was underthrust below the accretionary wedge. This is similar to what is seen in seismic profiles from the Nankai (Bangs et al., 2006) and Hikurangi margins (Bell et al., 2010), which show a décollement with a step-up caused by seamount subduction.

Another effect of seamount subduction in Exp. B is that raising the backstop widened the subduction channel, allowing thick layers of sand to subduct below the backstop through the subduction channel. In nature, if an oceanic plate with sufficiently large topographic highs subducts under a static backstop (cf. Tsuji et al., 2015), trench-fill terrigenous sediment accompanying the highs could be transported through the subduction channel to a higher-pressure environment than sediment on a smooth oceanic plate. Exp. B could be analogous to the transport mechanism of the protolith of the ancient Sanbagawa Metamorphic and Shimanto Accretionary complexes of southwestern Japan.

We propose a schematic model for the subduction of terrigenous sediment under an accretionary wedge (Figure 8). A progressive thickening of the wedge increases the overburden on the décollement that develops along weak layers in the cover sediment deposited on the subducting oceanic plate. This overburden results in dewatering and diagenetic alteration of the subducting sediment, which increases its mechanical strength, leading to a step-down in the décollement (Figure 8a, b). The reduction of sediment outflux due to narrowing of the subduction channel increases the mass of sediment underplated beneath the wedge and the rate of frontal accretion. When a topographic high (e.g., a seamount or an aseismic ridge) subducts under the wedge, the décollement steps up to the forethrust along the leading flank of the seamount (Figure 8b). This likely enables the subduction of terrigenous sediment beneath the wedge. Further subduction of the topographic high would raise the backstop and open the subduction channel for terrigenous sediment to be subducted into a high-pressure environment (Figure 8c). After the topographic high passes the inner wedge or backstop, the décollement under the accretionary wedge returns to the plate boundary or a weak layer within the trench-fill sediments.

Further Implications

Excess pore pressure is important in maintaining subduction channels along the plate interface (e.g., Saffer and Bekins, 2006). If the excess pore pressure drops below the overburden pressure, the physical conditions in the subduction channel may resemble those in the accretionary wedge (cf., Nankai and Barbados; Saffer, 2003). This probably accelerates both the stepping down of the décollement and underplating (Strasser et al., 2009; Kimura et al., 2011). In contrast, numerical simulations predict that the raising of the wedge due to the subduction of a seamount could delay the release of fluid from subducting sediment (Baba et al., 2001; Ruh et al., 2016). Low-velocity layers observed in the wake of subducting seamounts could provide evidence of under-compacted sediment with potentially high excess pore pressures (e.g., Sage et al., 2006). Furthermore, the seismic reflection characteristics of the Hikurangi subduction margin also suggest localized reductions in effective stress associated with seamount subduction (Bell et al., 2010). In addition to topographic relief, excess pore pressure could allow subduction channels to persist for longer than would otherwise be possible. Our experiments cannot currently incorporate the effects of excess pore pressure; consequently, we need to consider ways to include these effects.

Where the trench-fill sediments are insufficient to fully cover the topographic relief of the subducting oceanic crust, tectonic erosion may dominate and the accretionary wedge cannot grow, as seen in northeastern Japan, Costa Rica, and Ecuador (von Huene et al., 2004; Collot et al., 2011). Therefore, a sediment-rich subduction zone is required for terrigenous sediments to be transported from shallow depths (e.g., the Shimanto accretionary complex) to the depth of HP metamorphism (e.g., the Sanbagawa metamorphic complex).

CONCLUSIONS

We conducted a series of analogue experiments to investigate how terrigenous sediment is subducted under an accretionary wedge. The results yielded the following conclusions.

1. An increase in overburden stress due to progressive thickening of the accretionary wedge leads the décollement to step down and narrows the subduction channel. This accelerates the growth of the wedge through underplating and frontal accretion.

2. When a topographic high subducts under the wedge, the décollement steps up from a weak detachment layer within the incoming sediment to the forethrust along the landward flank of the seamount. This enables terrigenous sediment in the wake of the seamount to be underthrust beneath the wedge.

3. If a topographic high is rigid enough to uplift the backstop, it can widen the subduction channel to transport the terrigenous sediment that follows toward deeper environments.

4. A sufficient sediment supply to the trench and a rough oceanic crust surface are necessary for simultaneous shallow accretion, underplating of the wedge, and transportation of sediment to deeper settings as the protolith of HP–LT metamorphic rocks.

ACKNOWLEDGMENTS

We are grateful to Takato Takemura for useful suggestions regarding experimental material and Yujiro Ogawa for discussions about sediment subduction and accretion. This work was funded by a Grant-in-Aid from the Japan Society for the Promotion of Science (17K05687). This research was supported by the Cooperative Program (No. 143, 2017; No. 147, 2018; No. 151, 2019) of the Atmosphere and Ocean Research Institute, The University of Tokyo. Relevant multimedia data files for this study are available on Figshare (http://doi.org/10.6084/m9.figshare.10263674).

REFERENCES CITED

Albert, F., Kukowski, N., Tassara, A., and Oncken, O., 2018, Material transfer and subduction channel segmentation at erosive continental margins: Insights from scaled analogue experiments: Tectonophysics, v. 749, p. 46–61, https://doi.org/10.1016/j.tecto.2018.10.019.

Angiboust, S., Cambeses, A., Hyppolito, T., Glodny, J., Monié, P., Calderón, M., and Juliani, C., 2018, A 100-m.y.-long window onto mass-flow processes in the Patagonian Mesozoic subduction zone (Diego de Almagro Island, Chile): Geological Society of America Bulletin, v. 130, no. 9–10, p. 1439–1456, https://doi.org/10.1130/B31891.1.

Aoki, K., Iizuka, T., Hirata, T., Maruyama, S., and Terabayashi, M., 2007, Tectonic boundary between the Sanbagawa belt and the Shimanto belt in central Shikoku, Japan: Journal of the Geological Society of Japan, v. 113, no. 5, p. 171–183, https://doi.org/10.5575/geosoc.113.171.

Aoki, K., Isozaki, Y., Yamamoto, S., Maki, K., Yokoyama, T., and Hirata, T., 2012, Tectonic erosion in a Pacific-type orogen: Detrital zircon response to Cretaceous tectonics in Japan: Geology, v. 40, no. 12, p. 1087–1090, https://doi.org/10.1130/G33414.1.

Baba, T., Hori, T., Hirano, S., Cummins, P.R., Park, J.O., Kameyama, M., and Kaneda, Y., 2001, Deformation of a seamount subducting beneath an accretionary prism:

Constraints from numerical simulation: Geophysical Research Letters, v. 28, no. 9, p. 1827–1830, https://doi.org/10.1029/2000GL012266.

Bangs, N.L.B., Gulick, S.P.S., and Shipley, T.H., 2006, Seamount subduction erosion in the Nankai Trough and its potential impact on the seismogenic zone: Geology, v. 34, no. 8, p. 701–704, https://doi.org/10.1130/G22451.1.

Barker, D.H.N., Sutherland, R., Henrys, S., and Bannister, S., 2009, Geometry of the Hikurangi subduction thrust and upper plate, North Island, New Zealand: Geochemistry, Geophysics, Geosystems, v. 10, no. Q02007, https://doi.org/10.1029/2008GC002153.

Bell, R., Sutherland, R., Barker, D.H.N., Henrys, S., Bannister, S., Wallace, L., and Beavan, J., 2010, Seismic reflection character of the Hikurangi subduction interface, New Zealand, in the region of repeated Gisborne slow slip events: Geophysical Journal International, v. 180, no. 1, p. 34–48, https://doi.org/10.1111/j.1365-246X.2009.04401.x.

Booth-Rea, G., Klaeschen, D., Grevemeyer, I., and Reston, T., 2008, Heterogeneous deformation in the Cascadia convergent margin and its relation to thermal gradient (Washington, NW USA): Tectonics, v. 27, no. TC4005, https://doi.org/10.1029/2007TC002209.

Buiter, S.J.H., 2012, A review of brittle compressional wedge models: Tectonophysics, v. 530–531, p. 1–17, https://doi.org/10.1016/j.tecto.2011.12.018.

Calvert, A.J., Preston, L.A., and Farahbod, A.M., 2011, Sedimentary underplating at the Cascadia mantle-wedge corner revealed by seismic imaging: Nature Geoscience, v. 4, no. 8, p. 545–548, https://doi.org/10.1038/ngeo1195.

Collot, J.Y., Agudelo, W., Ribodetti, A., and Marcaillou, B., 2008, Origin of a crustal splay fault and its relation to the seismogenic zone and underplating at the erosional north Ecuador–south Colombia oceanic margin: Journal of Geophysical Research, v. 113, no. B12102, https://doi.org/10.1029/2008JB005691.

Collot, J.Y., Ribodetti, A., Agudelo, W., and Sage, F., 2011, The South Ecuador subduction channel: Evidence for a dynamic mega-shear zone from 2D fine-scale seismic reflection imaging and implications for material transfer: Journal of Geophysical Research, v. 116, no. B11, https://doi.org/10.1029/2011JB008429.

Dahlen, F.A., 1984, Noncohesive critical coulomb wedges: An exact solution: Journal of Geophysical Research, v. 89, no. B12, p. 10,125–10,133, https://doi.org/10.1029/JB089iB12p10125.

Deng, X., and Underwood, M.B., 2001, Abundance of smectite and the location of a plate-boundary fault, Barbados accretionary prism: Geological Society of America Bulletin, v. 113, no. 4, p. 495–507, https://doi.org/10.1130/0016-7606(2001)113<0495:AOSATL>2.0.CO;2.

Dominguez, S., Malavieille, J., and Lallemand, S.E., 2000, Deformation of accretionary wedges in response to seamount subduction: Insights from sandbox experiments: Tectonics, v. 19, no. 1, p. 182–196, https://doi.org/10.1029/1999TC900055.

Dotare, T., Yamada, Y., Adam, J., Hori, T., and Sakaguchi, H., 2016, Initiation of a thrust fault revealed by analog experiments: Tectonophysics, v. 684, p. 148–156, https://doi.org/10.1016/j.tecto.2015.12.023.

Dumitru, T.A., Ernst, W.G., Hourigan, J.K., and McLaughlin, R.J., 2015, Detrital zircon U–Pb reconnaissance of the Franciscan subduction complex in northwestern California: International Geology Review, v. 57, no. 5–8, p. 767–800, https://doi.org/10.1080/00206814.2015.1008060.

Ernst, W.G., 2011, Accretion of the Franciscan Complex attending Jurassic–Cretaceous geotectonic development of northern and central California: Geological Society of America Bulletin, v. 123, no. 9–10, p. 1667–1678, https://doi.org/10.1130/B30398.1.

Geological Survey of Japan, AIST, ed., 2015, Seamless digital geological map of Japan 1:200,000, May 29, 2015 version: Geological Survey of Japan, National Institute of Advanced Industrial Science and Technology, [Cited 06 Dec 2019]. Available from: https://gbank.gsj.jp/seamless/index_en.html.

Ghisetti, F.C., Barnes, P.M., Ellis, S., Plaza-Faverola, A.A., and Barker, D.H.N., 2016, The last 2 Myr of accretionary wedge construction in the central Hikurangi margin (North Island, New Zealand): Insights from structural modeling: Geochemistry, Geophysics, Geosystems, v. 17, p. 2661–2686, https://doi.org/10.1002/2016GC006341.

Glodny, J., Lohrmann, J., Echtler, H., Gräfe, K., Seifert, W., Collao, S., and Figueroa, O., 2005, Internal dynamics of a paleoaccretionary wedge: insights from combined isotope tectonochronology and sandbox modelling of the South-Central Chilean forearc: Earth and Planetary Science Letters, v. 231, no. 1, p. 23–39, https://doi.org/10.1016/j.epsl.2004.12.014.

Graveleau, F., Malavieille, J., and Dominguez, S., 2012, Experimental modelling of orogenic wedges: A review: Tectonophysics, v. 538–540, p. 1–66, https://doi.org/10.1016/j.tecto.2012.01.027.

Gulick, S.P.S., Meltzer, A.M., and Clarke, S.H., 1998, Seismic structure of the southern Cascadia subduction zone and accretionary prism north of the Mendocino triple junction: Journal of Geophysical Research, v. 103, no. B11, p. 27,207–27,222, https://doi.org/10.1029/98JB02526.

Hara, H., and Hara, K., 2019, Radiolarian and U–Pb zircon dating of Late Cretaceous and Paleogene Shimanto accretionary complexes, Southwest Japan: Temporal variations in provenance and offset across an out-of-sequence thrust: Journal of Asian Earth Sciences, v. 170, p. 29–44, https://doi.org/10.1016/j.jseaes.2018.10.016.

Hara, H., Nakamura, Y., Hara, K., Kurihara, T., Mori, H., Iwano, H., Danhara, T., Sakata, S., and Hirata, T., 2017, Detrital zircon multi-chronology, provenance, and low-grade metamorphism of the Cretaceous Shimanto accretionary complex, eastern Shikoku, Southwest Japan: Tectonic evolution in response to igneous activity within a subduction zone: Island Arc, v. 26, no. 6, p. e12,218, https://doi.org/10.1111/iar.12218.

Hubbert, M.K., 1937, Theory of scale models as applied to the study of geologic structures: Geological Society of America Bulletin, v. 48, no. 10, p. 1459–1519, https://doi.org/10.1130/GSAB-48-1459.

Huot, G., and Singh, S.C., 2018, Seismic evidence for fluid/gas beneath the Mentawai Fore-Arc Basin, central Sumatra: Journal of Geophysical Research: Solid Earth, v. 123, no. 2, p. 957–976, https://doi.org/10.1002/2017JB014849.

Jacobson, C.E., Grove, M., Pedrick, J.N., Barth, A.P., Marsaglia, K.M., Gehrels, G.E., and Nourse, J.A., 2011, Late Cretaceous–early Cenozoic tectonic evolution of the southern California margin inferred from provenance of trench and forearc sediments: Geological Society of America Bulletin, v. 123, no. 3–4, p. 485–506, https://doi.org/10.1130/B30238.1.

Jordan, T.H., Menard, H.W., and Smith, D.K., 1983, Density and size distribution of seamounts in the eastern Pacific inferred from wide-beam sounding data: Journal of Geophysical Research, v. 88, no. B12, p. 10,508–10,518, https://doi.org/10.1029/JB088iB12p10508.

Kiminami, K., Hamasaki, A., and Matsuura, T., 1999, Geochemical contrast between the Sanbagawa psammitic schists (Oboke unit) and the Cretaceous Shimanto sandstones in Shikoku, Southwest Japan and its geologic significance: Island Arc, v. 8, no. 3, p. 373–382, https://doi.org/10.1046/j.1440-1738.1999.00248.x.

Kimura, G., Kitamura, Y., Hashimoto, Y., Yamaguchi, A., Shibata, T., Ujiie, K., and Okamoto, S., 2007, Transition of accretionary wedge structures around the up-dip limit of the seismogenic subduction zone: Earth and Planetary Science Letters, v. 255, no. 3–4, p. 471–484, https://doi.org/10.1016/j.epsl.2007.01.005.

Kimura, G., Moore, G.F., Strasser, M., Screaton, E., Curewitz, D., Streiff, C., and Tobin, H., 2011, Spatial and temporal evolution of the megasplay fault in the Nankai Trough: Geochemistry, Geophysics, Geosystems, v. 12, no. Q0A008, https://doi.org/10.1029/2010GC003335.

Kimura, H., Takeda, T., Obara, K., and Kasahara, K., 2010, Seismic evidence for active underplating below the megathrust earthquake zone in Japan: Science, v. 329, no. 5988, p. 210–212, https://doi.org/10.1126/science.1187115.

Kopp, H., Hindle, D., Klaeschen, D., Oncken, O., Reichert, C., and Scholl, D., 2009, Anatomy of the western Java plate interface from depth-migrated seismic images: Earth and Planetary Science Letters, v. 288, no. 3–4, p. 399–407, https://doi.org/10.1016/j.epsl.2009.09.043.

Kukowski, N., von Huene, R., Malavieille, J., and Lallemand, S.E., 1994, Sediment accretion against a buttress beneath the Peruvian continental margin at 12° S as simulated with sandbox modeling: Geologische Rundschau, v. 83, no. 4, p. 822–831, https://doi.org/10.1007/BF00251079.

Lallemand, S.E., Malavieille, J., and Calassou, S., 1992, Effects of oceanic ridge subduction on accretionary wedges; experimental modeling and marine observations: Tectonics, v. 11, no. 6, p. 1301–1313, https://doi.org/10.1029/92TC00637.

Lallemand, S.E., Schnürle, P., and Malavieille, J., 1994, Coulomb theory applied to accretionary and nonaccretionary wedges: Possible causes for tectonic erosion and/or frontal accretion: Journal of Geophysical Research, v. 99, no. B6, p. 12,033–12,055, https://doi.org/10.1029/94JB00124.

Li, J., Shillington, D.J., Saffer, D.M., Bécel, A., Nedimović, M.R., Kuehn, H., Webb, S.C., Keranen, K.M., and Abers, G.A., 2018, Connections between subducted sediment, pore-fluid pressure, and earthquake behavior along the Alaska megathrust: Geology, v. 46, no. 4, p. 299–302, https://doi.org/10.1130/G39557.1.

Lohrmann, J., Kukowski, N., Adam, J., and Oncken, O., 2003, The impact of analogue material properties on the geometry, kinematics, and dynamics of convergent sand wedges: Journal of Structural Geology, v. 25, no. 10, p. 1691–1711, https://doi.org/10.1016/S0191-8141(03)00005-1.

Melnick, D., Bookhagen, B., Echtler, H.P., and Strecker, M.R., 2006, Coastal deformation and great subduction earthquakes, Isla Santa María, Chile (37°S): Geological Society of America Bulletin, v. 118, no. 11–12, p. 1463–1480, https://doi.org/10.1130/B25865.1.

Milliman, J.D., and Syvitski, J.P.M., 1992, Geomorphic/tectonic control of sediment discharge to the ocean: The importance of small mountainous rivers: Journal of Geology, v. 100, no. 5, p. 525–544, https://doi.org/10.1086/629606.

Moore, G.F., Kanagawa, K., Strasser, M., Dugan, B., Maeda, L., Toczko, S., and the IODP Expedition 338 Scientific Party, 2014, IODP Expedition 338: NanTroSEIZE Stage 3: NanTroSEIZE plate boundary deep riser 2: Scientific Drilling, v. 17, p. 1–12, https://doi.org/10.5194/sd-17-1-2014.

Moore, G.F., Zhao, Z., Shipley, T.H., Bangs, N., and Moore, J.C., 1995, Structural setting of the Leg 156 area, northern Barbados Ridge accretionary prism, *in* Shipley, T.H., Ogawa, Y., Blum, P., and et al., eds., Proceedings of the Ocean Drilling Program, Initial Reports, v. 156: College Station, TX, Ocean Drilling Program, p. 13–27, https://doi.org/10.2973/odp.proc.ir.156.102.1995.

Moore, G.F., others, Klaus, A., and Becker, L., 2001, New insights into deformation and fluid flow processes in the Nankai Trough accretionary prism: Results of Ocean Drilling Program Leg 190: Geochemistry, Geophysics, Geosystems, v. 2, no. 1058, https://doi.org/10.1029/2001GC000166.

Moore, J.C., 1975, Selective subduction: Geology, v. 3, no. 9, p. 530–532, https://doi.org/10.1130/0091-7613(1975)3<530:SS>2.0.CO;2.

Moore, J.C., others, Fisher, M.A., and Sample, J., 1991, EDGE deep seismic reflection transect of the eastern Aleutian arc-trench layered lower crust reveals underplating and continental growth: Geology, v. 19, no. 5, p. 420–424, https://doi.org/10.1130/0091-7613(1991)019<0420:EDSRTO>2.3.CO;2.

Moore, J.C., Plank, T.A., Chester, F.M., Polissar, P.J., and Savage, H.M., 2015, Sediment provenance and controls on slip propagation: Lessons learned from the 2011 Tohoku and other great earthquakes of the subducting northwest Pacific plate: Geosphere, v. 11, no. 3, p. 533–541, https://doi.org/10.1130/GES01099.1.

Morgan, J.K., and Bangs, N.L., 2017, Recognizing seamount-forearc collisions at accretionary margins: Insights from discrete numerical simulations: Geology, v. 45, no. 7, p. 635–638, https://doi.org/10.1130/G38923.1.

Nagata, M., Miyazaki, K., Iwano, H., Danhara, T., Obayashi, H., Hirata, T., Yagi, K., Kouchi, Y., Yamamoto, K., and Otoh, S., 2019, Timescale of material circulation in subduction zone: U–Pb zircon and K–Ar phengite double-dating of the Sanbagawa metamorphic complex in the Ikeda district, central Shikoku, southwest Japan: Island Arc, v. 28, no. 4, p. e12,306, https://doi.org/10.1111/iar.12306.

Noda, A., 2016, Forearc basins: Types, geometries, and relationships to subduction zone dynamics: Geological Society of America Bulletin, v. 128, no. 5–6, p. 879–895, https://doi.org/10.1130/B31345.1.

Noda, A., Danhara, T., Iwano, H., and Hirata, T., 2017, LA-ICP-MS U–Pb and fission-track ages of felsic tuff beds of the Takikubo Formation, Izumi Group in the Kan-onji district, eastern Shikoku, southwestern Japan: Bulletin of the Geological Survey of Japan, v. 68, no. 3, p. 119–130, https://doi.org/10.9795/bullgsj.68.119.

Noda, A., and Sato, D., 2018, Submarine slope–fan sedimentation in an ancient forearc related to contemporaneous magmatism: The Upper Cretaceous Izumi Group, southwestern Japan: Island Arc, v. 27, no. 2, p. e12,240, https://doi.org/10.1111/iar.12240.

Okay, A.I., Tüysüz, O., Satır, M., Özkan-Altiner, S., Altiner, D., Sherlock, S., and Eren, R.H., 2006, Cretaceous and Triassic subduction-accretion, high-pressure–low-temperature metamorphism, and continental growth in the Central Pontides, Turkey: Geological Society of America Bulletin, v. 118, no. 9–10, p. 1247–1269, https://doi.org/10.1130/B25938.1.

Otoh, S., Shimojo, M., Aoki, K., Nakama, T., Maruyama, S., and Yanai, S., 2010, Age distribution of detrital zircons in the psammitic schist of the Sanbagawa Belt, Southwest Japan: Journal of Geography (Chigaku Zasshi), v. 119, no. 2, p. 333–346, https://doi.org/10.5026/jgeography.119.333.

Park, J.O., Tsuru, T., Takahashi, N., Hori, T., Kodaira, S., Nakanishi, A., Miura, S., and Kaneda, Y., 2002, A deep strong reflector in the Nankai accretionary wedge from multichannel seismic data: Implications for underplating and interseismic shear stress release: Journal of Geophysical Research, v. 107, no. B4, https://doi.org/10.1029/2001JB000262.

Plafker, G., Moore, J.C., and Winkler, G.R., 1994, Geology of the Southern Alaska margin, *in* Plafker, G., and Berg, H.C., eds., The geology of Alaska, The Geology of North America, v. G–1: chap. 12, Boulder, Colorado, United States, Geological Society of America, p. 389–449, https://doi.org/10.1130/DNAG-GNA-G1.389.

Plaza-Faverola, A., Henrys, S., Pecher, I., Wallace, L., and Klaeschen, D., 2016, Splay fault branching from the Hikurangi subduction shear zone: Implications for slow slip and fluid flow: Geochemistry, Geophysics, Geosystems, v. 17, p. 5009–5023, https://doi.org/10.1002/2016GC006563.

Raymond, L.A., 2018, What is Franciscan?: revisited: International Geology Review, v. 60, no. 16, p. 1968–2030, https://doi.org/10.1080/00206814.2017.1396933.

Ruh, J.B., Sallarès, V., Ranero, C.R., and Gerya, T., 2016, Crustal deformation dynamics and stress evolution during seamount subduction: High-resolution 3-D numerical modeling: Journal of Geophysical Research: Solid Earth, v. 121, p. 6880–6902, https://doi.org/10.1002/2016JB013250.

Saffer, D.M., 2003, Pore pressure development and progressive dewatering in underthrust sediments at the Costa Rican subduction margin: Comparison with northern Barbados and Nankai: Journal of Geophysical Research, v. 108, no. B5, 2261, https://doi.org/10.1029/2002JB001787.

Saffer, D.M., and Bekins, B.A., 2006, An evaluation of factors influencing pore pressure in accretionary complexes; implications for taper angle and wedge mechanics: Journal of Geophysical Research, v. 111, no. B04101, https://doi.org/10.1029/2005JB003990.

Sage, F., Collot, J.Y., and Ranero, C.R., 2006, Interplate patchiness and subduction-erosion mechanisms: Evidence from depth-migrated seismic images at the central Ecuador convergent margin: Geology, v. 34, no. 12, p. 997–1000, https://doi.org/10.1130/G22790A.1.

Sample, J.C., and Moore, J.C., 1987, Structural style and kinematics of an underplated slate belt, Kodiak and adjacent islands, Alaska: Geological Society of America Bulletin, v. 99, no. 1, p. 7–20, https://doi.org/10.1130/0016-7606(1987)99<7:SSAKOA>2.0.CO;2.

Schellart, W.P., 2000, Shear test results for cohesion and friction coefficients for different granular materials: scaling implications for their usage in analogue modelling: Tectonophysics, v. 324, no. 1–2, p. 1–16, https://doi.org/10.1016/S0040-1951(00)00111-6.

Schellart, W.P., and Strak, V., 2016, A review of analogue modelling of geodynamic processes: Approaches, scaling, materials and quantification, with an application to subduction experiments: Journal of Geodynamics, v. 100, p. 7–32, https://doi.org/10.1016/j.jog.2016.03.009.

Scholl, D.W., 2019, Seismic imaging evidence that forearc underplating built the accretionary rock record of coastal North and South America: Geological Magazine, v. ??, p. 1–14, https://doi.org/10.1017/S0016756819000955.

Schumann, K., Behrmann, J.H., Stipp, M., Yamamoto, Y., Kitamura, Y., and Lempp, C., 2014, Geotechnical behavior of mudstones from the Shimanto and Boso accretionary complexes, and implications for the Nankai accretionary prism: Earth, Planets and Space, v. 66, no. 1, p. 129, https://doi.org/10.1186/1880-5981-66-129.

Shibata, T., Orihashi, Y., Kimura, G., and Hashimoto, Y., 2008, Underplating of mélange evidenced by the depositional ages: U–Pb dating of zircons from the Shimanto accretionary complex, southwest Japan: Island Arc, v. 17, no. 3, p. 376–393, https://doi.org/10.1111/j.1440-1738.2008.00626.x.

Singh, S.C., others, Tapponnier, P., and Hananto, N.D., 2008, Seismic evidence for broken oceanic crust in the 2004 Sumatra earthquake epicentral region: Nature Geoscience, v. 1, no. 11, p. 777–781, https://doi.org/10.1038/ngeo336.

Smith, D.K., 1988, Shape analysis of Pacific seamounts: Earth and Planetary Science Letters, v. 90, no. 4, p. 457–466, https://doi.org/10.1016/0012-821X(88)90143-4.

Strasser, M., others, Kimura, G., and Kitamura, Y., 2009, Origin and evolution of a splay fault in the Nankai accretionary wedge: Nature Geoscience, v. 2, no. 9, p. 648–652, https://doi.org/10.1038/NGEO609.

Tsuji, T., Ashi, J., Strasser, M., and Kimura, G., 2015, Identification of the static backstop and its influence on the evolution of the accretionary prism in the Nankai Trough: Earth and Planetary Science Letters, v. 431, p. 15–25, https://doi.org/10.1016/j.epsl.2015.09.011.

Vannucchi, P., Remitti, F., and Bettelli, G., 2008, Geological record of fluid flow and seismogenesis along an erosive subducting plate boundary: Nature, v. 451, no. 7179, p. 699–703, https://doi.org/10.1038/nature06486.

von Huene, R., and Culotta, R., 1989, Tectonic erosion at the front of the Japan Trench convergent margin: Tectonophysics, v. 160, p. 75–90, https://doi.org/10.1016/0040-1951(89)90385-5.

von Huene, R., Ranero, C.R., and Vannucchi, P., 2004, Generic model of subduction erosion: Geology, v. 32, no. 10, p. 913–916, https://doi.org/10.1130/G20563.1.

Vrolijk, P., 1990, On the mechanical role of smectite in subduction zones: Geology, v. 18, no. 8, p. 703–707, https://doi.org/10.1130/0091-7613(1990)018<0703:OTMROS>2.3.CO;2.

Wallis, S., 1998, Exhuming the Sanbagawa metamorphic belt: the importance of tectonic discontinuities: Journal of Metamorphic Geology, v. 16, no. 1, p. 83–95, https://doi.org/10.1111/j.1525-1314.1998.00072.x.

Willner, A.P., Glodny, J., Gerya, T.V., Godoy, E., and Massonne, H.J., 2004, A counterclockwise PTt path of high-pressure/low-temperature rocks from the Coastal Cordillera accretionary complex of south-central Chile: constraints for the earliest stage of subduction mass flow: Lithos, v. 75, no. 3, p. 283–310, https://doi.org/10.1016/j.lithos.2004.03.002.

Yamada, Y., Baba, K., Miyakawa, A., and Matsuoka, T., 2014, Granular experiments of thrust wedges: Insights relevant to methane hydrate exploration at the Nankai accretionary prism: Marine and Petroleum Geology, v. 51, p. 34–48, https://doi.org/10.1016/j.marpetgeo.2013.11.008.

Yamada, Y., Kaneda, K., and Matsuoka, T., 2006, Influences of material properties on analogue model experiments of geologic structures: Journal of the Society of Materials Science, Japan, v. 55, no. 5, p. 452–457, https://doi.org/10.2472/jsms.55.452, in Japanese with English abstract.

Ye, S., Flueh, E.R., Klaeschen, D., and von Huene, R., 1997, Crustal structure along the EDGE transect beneath the Kodiak shelf off Alaska derived from OBH seismic refraction data: Geophysical Journal International, v. 130, no. 2, p. 283–302, https://doi.org/10.1111/j.1365-246X.1997.tb05648.x.

Table 1. Total sediment input and output, and their ratio. Asterisk (*) indicates output includes the volume of the seamount.

Exp.	Displacement (cm)	Input (cm^3)	Output* (cm^3)	Accretion (cm^3)	Output/Input Ratio
A	30.0	2,912	1,052	1,860	0.36
B	35.0	3,315	1,527	1,788	0.46

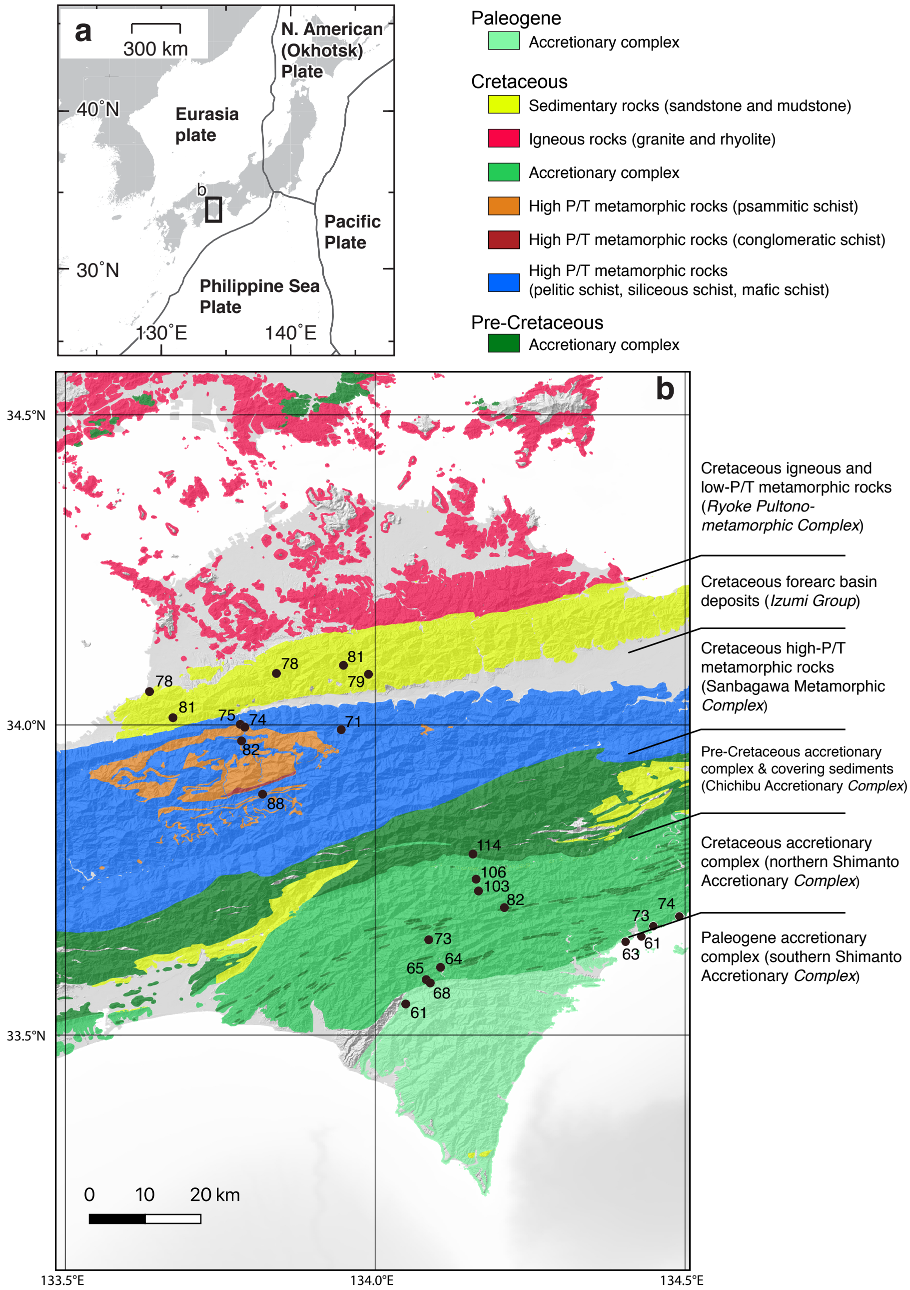

Figure 1. Generalized geological map of eastern Shikoku, southwestern Japan, reproduced from the Seamless Digital Geological Map of Japan (Geological Survey of Japan, AIST, 2015). Black dots are labeled with detrital zircon U–Pb ages (Ma) of felsic tuff beds in the Izumi Group, composed mainly of sandy turbidites and mudstone (Noda et al., 2017; **?**), the psammitic schist of the Sanbagawa Metamorphic Complex (Aoki et al., 2007; Nagata et al., 2019; Otoh et al., 2010), and sandy turbidites in the northern Shimanto Accretionary Complex (Hara et al., 2017; Hara and Hara, 2019; Shibata et al., 2008).

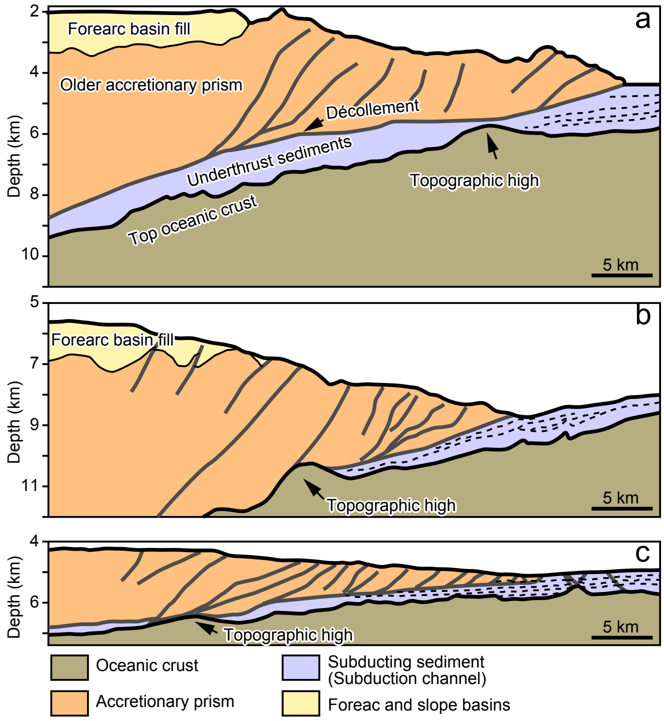

Figure 2. Representative cross-sections of accretionary margins with topographic highs. (a) Nankai Trough (Moore et al., 2014). (b) Southwestern Alaskan margin (Li et al., 2018). (c) Northern Barbados margin (Moore et al., 1995).

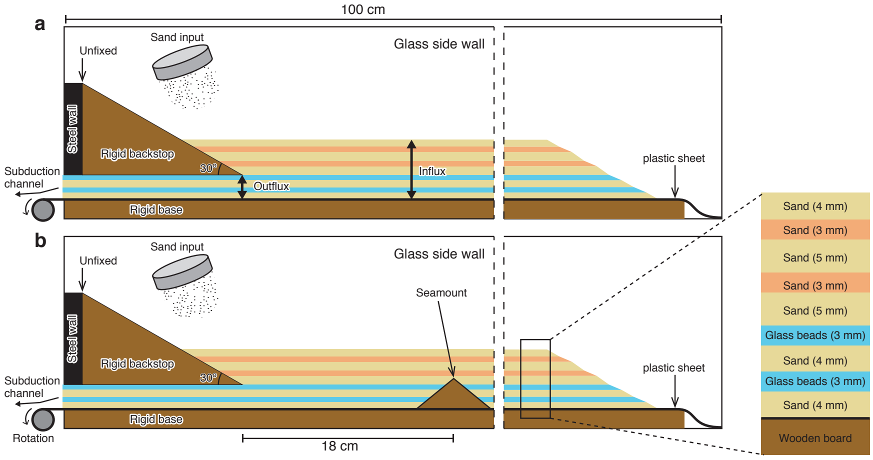

Figure 3. Experimental apparatus.

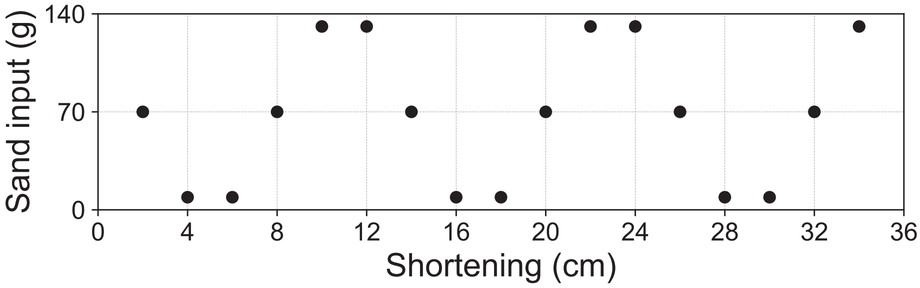

Figure 4. Amount of sand added to the topographic lows during the experiments.

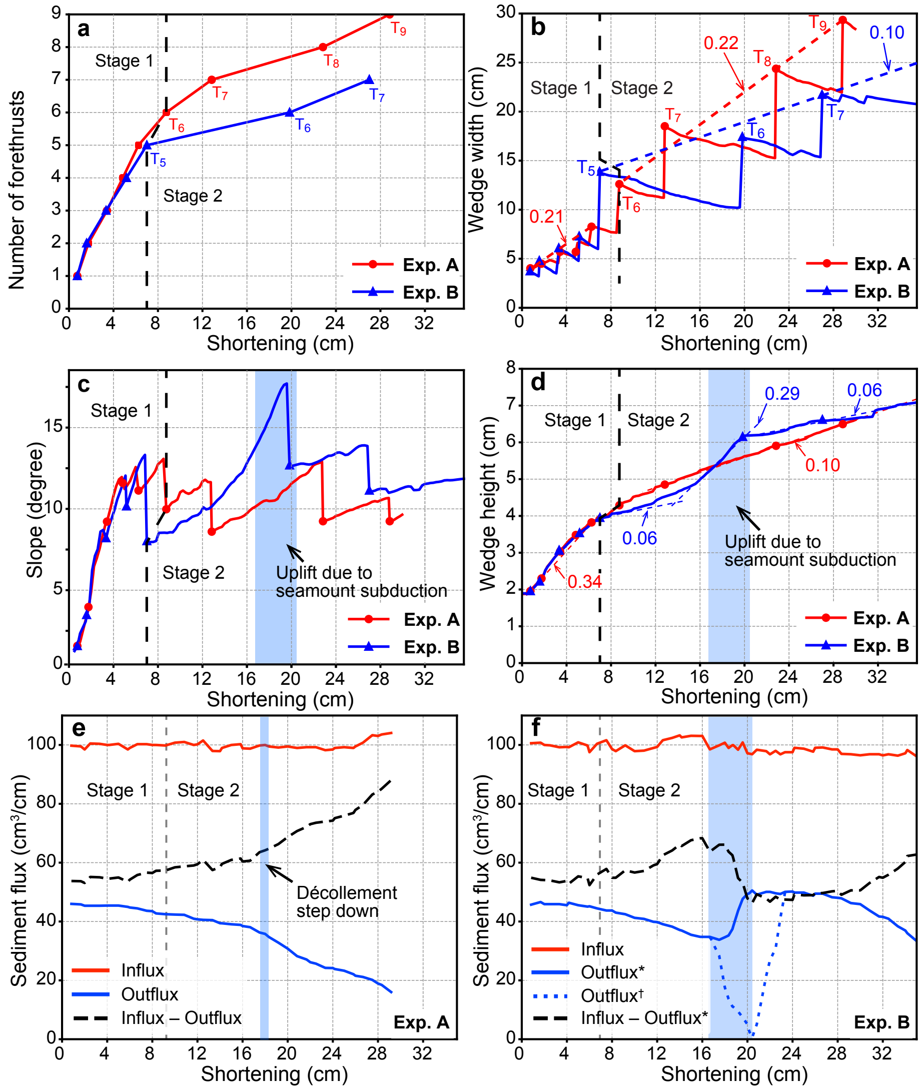

Figure 5. Geomorphic parameters of the wedges (a–d) and sediment fluxes (e–f). (a) Number of forethrusts. (b) Wedge width. Dashed lines are labelled with wedge progradation rates calculated from the amount of progradation (cm) divided by the amount of shortening (cm). (c) Wedge slope angle. (d) Wedge height. Dashed lines are labelled with uplift rates calculated from the amount of uplift (cm) divided by the amount of shortening (cm). (e) Sediment influx and outflux for Exp. A (without seamount). (f) Sediment influx and outflux for Exp. B (with seamount). Asterisk (*) and dagger (†) indicate outfluxes including and excluding the volume of the seamount, respectively.

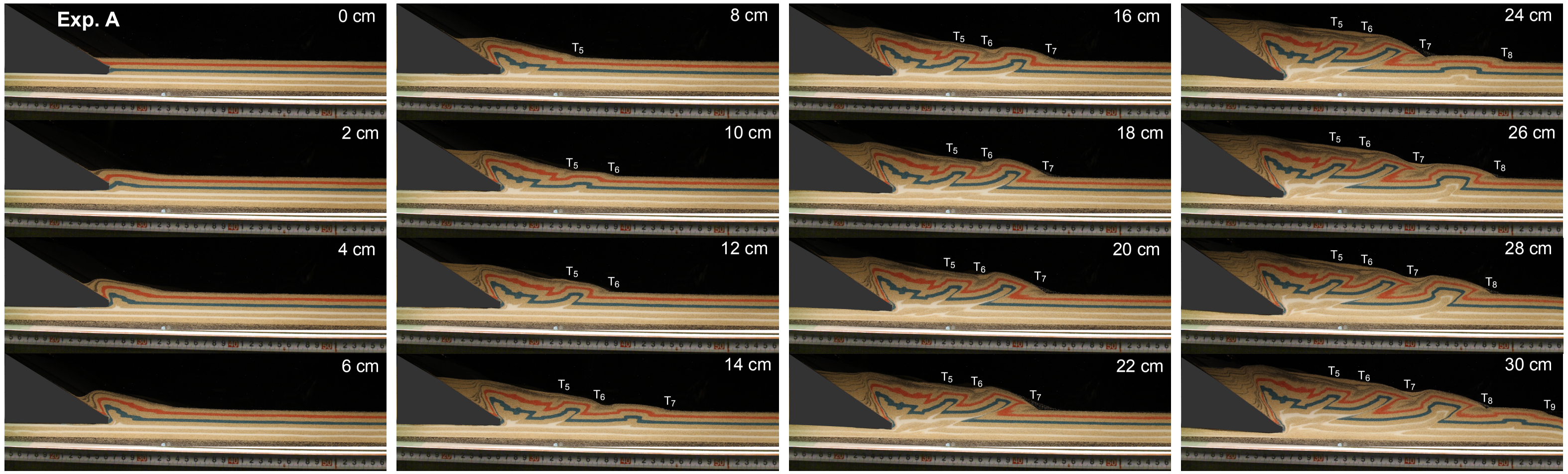

Figure 6. Representative images of Exp. A.

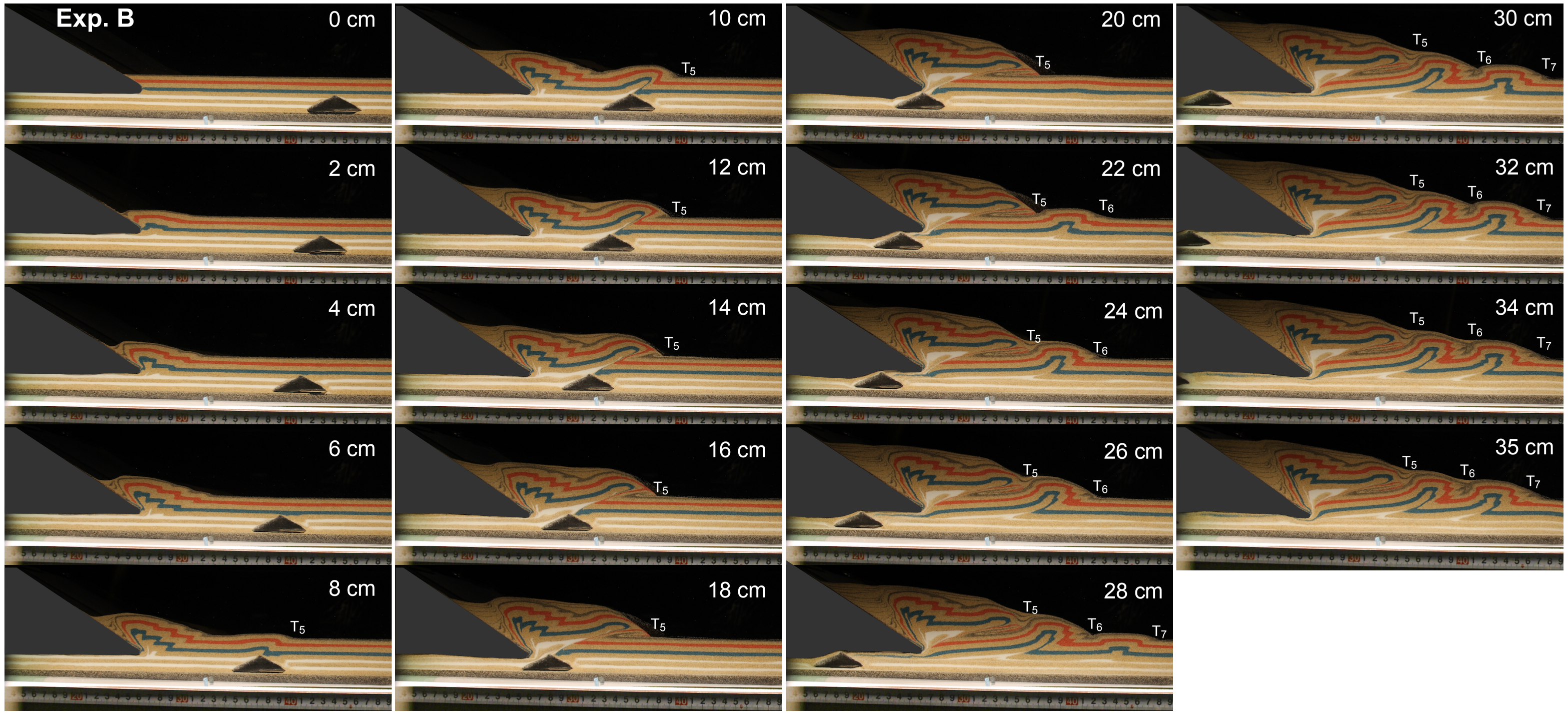

Figure 7. Representative images of Exp. B.

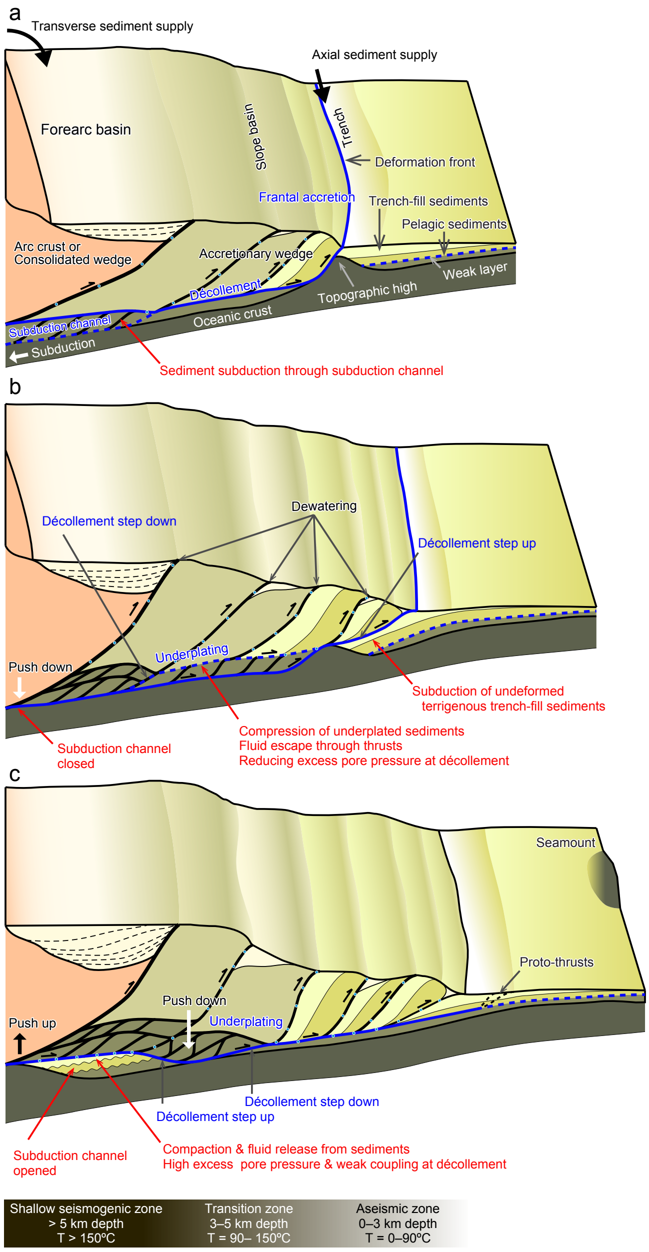

Figure 8. Schematic model of sediment subduction through a subduction channel beneath an accretionary wedge. (a) Subduction of a topographic high raises the décollement to accommodate the topographic high and the following trench-fill sediment. (b) An increase in overburden gravitational force under the inner wedge shifts the décollement downward and facilitates underplating. In the wake of the subducting seamount, terrigenous sediment is underthrust beneath the accretionary wedge. (c) The seamount raises the backstop, enabling the subduction of terrigenous sediment. After the passage of the seamount, the décollement returns to the original, lower position, and the subduction channel closes, resulting in underplating beneath the wedge.